The Effect of the Endothelial Cell Cortex on Atomic Force Microscopy Measurements

R. Vargas-Pinto,[†] H. Gong,[‡] A. Vahabikashi,[†] and M. Johnson[§*]

[†]Biomedical Engineering Department, Northwestern University, Evanston, Illinois; [‡]Department of Ophthalmology, Boston University School of Medicine, Boston, Massachusetts; and [§]Departments of Biomedical Engineering, Mechanical Engineering and Ophthalmology, Northwestern University, Evanston, Illinois

ABSTRACT We examined whether the presence of the cell cortex might explain, in part, why previous studies using atomic force microscopy (AFM) to measure cell modulus (E) gave higher values with sharp tips than for larger spherical tips. We confirmed these AFM findings in human umbilical vein endothelial cells (HUVEC) and Schlemm's canal (SC) endothelial cells with AFM indentation $\leq$ 400 nm, two cell types with prominent cortices (312 $\pm$ 65 nm in HUVEC and 371 $\pm$ 91 nm in SC cells). With spherical tips, E (kPa) was 0.71 $\pm$ 0.16 in HUVEC and 0.94 $\pm$ 0.06 in SC cells. Much higher values of E were measured using sharp tips: 3.23 $\pm$ 0.54 in HUVEC and 6.67 $\pm$ 1.07 in SC cells. Previous explanations for this difference such as strain hardening or a substrate effect were shown to be inconsistent with our measurements. Finite element modeling studies showed that a stiff cell cortex could explain the results. In both cell types, Latrunculin-A greatly reduced E for sharp and rounded tips, and also reduced the ratio of the values measured with a sharp tip as compared to a rounded tip. Our results suggest that the cell cortex increases the apparent endothelial cell modulus considerably when measured using a sharp AFM tip.

INTRODUCTION

AFM is widely used to characterize the elasticity of living cells (1–7). As the tip mounted at the end of a cantilever indents the cell, the deflection of the cantilever is measured and converted into force. The resulting force-versus-indentation relationship can be used to determine a measure of aggregate cell modulus. There are different tip geometries available including sharp pyramidal tips and spherical tips, and corresponding to these different geometries are different Hertzian models that can be used to calculate the Young's modulus based on the force-versus-indentation relationship (8).

Stolz et al. (9) measured the Young's modulus of agarose gels using spherical (radius of 2.5 μm) and sharp pyramidal tips (radius of 20 nm) and found the same average modulus using both tips. Similarly, Engler et al. (10) found no statistical difference in the elastic modulus measured with pyramidal and spherical tips when probing thick samples of polyacrylamide gels. However, a variety of studies have reported that AFM measurements on living cells using sharp tips yield significantly higher values of modulus than those measured using larger spherical probes (11–14).

The reason that sharp tips give higher estimates of cell modulus than spherical tips remains controversial. Several studies have shown that some of these differences can be attributed to artifacts in the measurement process including strain stiffening (12,15,16), contact point determination (15), contact area uncertainty (11), and substrate interactions (15–17). Many of these artifacts would be expected to be enhanced by deeper indentations. Harris and Charras (11) suggested that indentations should be held to <600 nm.

Several groups have used such shallow indentations and found that AFM measurements on cells using sharp tips still yield significantly higher values of modulus than those measured using larger spherical probes. Rico et al. (13) measured the stiffness of alveolar epithelial cells with indentations as small as 200 nm and found that AFM measurements with sharp tips were roughly twice as high as those with spherical tips on these cells. Ng et al. (18) made AFM measurements on chondrocytes and also found that the cell stiffness, as measured by a sharp AFM tip, was also approximately twice as high was as when measured with a spherical tip. (We note that there is an error in Eq. A1 of Ng et al. (18) and in the reported value of E for the sharp tip that we have confirmed with the authors.)

We used AFM to determine the Young's modulus (E) of human umbilical vein endothelial cells (HUVEC) and cells from the inner wall endothelium of Schlemm's Canal (SC) in the eye. The mechanical characteristics of the latter are of interest to the study of glaucoma where an increased stiffness of these cells is associated with an increased resistance to the outflow of aqueous humor from the eye (19,20). We used shallow indentations (δ < 400 nm) to minimize possible artifacts, along with an algorithm for contact point determination (21). We also examined the effects of increased indentation within this range to further rule the possibility of AFM artifacts (16). We found that in these cell types, the cell moduli as measured with sharp pyramidal tips was higher than those measured with larger spherical tips. We explored what might be the biophysical causes of the elevated modulus values measured using a sharp AFM

Submitted August 6, 2012, and accepted for publication May 13, 2013.

*Correspondence: m-johnson2@northwestern.edu

Editor: Daniel Muller.

0006-3495/13/07/0300/10 $2.00

http://dx.doi.org/10.1016/j.bpj.2013.05.034

tip. We found that the cortex of these cells is likely responsible for this.

METHODS

Cell culture, fluorescent staining, and experiments with latrunculin

Endothelial cell growth medium and two human umbilical vein endothelial cell (HUVEC) strains were purchased from Cell Applications (San Diego, CA). Schlemm's Canal (SC) cells from six strains (each from a different donor), courtesy of Dr. W. Daniel Stamer (then at the Department of Ophthalmology, University of Arizona, Tucson, AZ), were isolated from enucleated eyes or corneal rims following previously described procedures (22). Eyes used for cell isolation had no history of eye disease, laser or anterior segment surgery. Culture medium used for SC cells was DMEM/Low glucose (Hyclone Laboratories, Logan, UT) with 10% fetal bovine serum (PAA Laboratories, New Bedford, MA) and 1% penicillin and streptomycin (Lonza, Walkersville, MD).

HUVEC and SC cells were maintained under normal culture conditions (37°C and 5% CO_2) and culture medium was changed three times per week. Cells used for experiments described here were passage 5 or less. In preparation for experiments, cells were detached from culture flasks using 0.25% trypsin with EDTA and plated in 60-mm petri dishes. The time during which cells remained in petri dishes before experimentation varied between 1 and 8 days for HUVEC and 2–13 days for SC cells. Cell culture supplies were purchased from VWR International (West Chester, PA) unless otherwise specified.

On the day of experimentation, subconfluent cells were stained with fluorescent dyes (Hoechst 33342, 3 μg/mL, and Calcein AM, 2 μg/mL, both purchased from Invitrogen, Carlsbad, CA) to assess cell viability, ensure that the cells were not punctured during the AFM measurement, and aid in localization of cell nucleus. After staining, cells were incubated for at least 1 h before beginning AFM experiments. The effects of cell staining were investigated in one HUVEC strain.

Additional experiments were done to examine the effect of Latrunculin, an actin depolymerizing agent, on cell modulus. A stock solution of 1 mM Latrunculin-A in dimethyl sulfoxide (both purchased from Sigma-Aldrich, St. Louis, MO) was further diluted in serum free culture medium to a final concentration of 1 μM. Cells already stained with fluorescent dyes were treated with Latrunculin-A for 30 min, washed, and then returned to media.

AFM measurements

AFM measurements were made using a BioScope-II with NanoscopeV controller and software (Veeco, Santa Barbara, CA) mounted over an inverted microscope (Carl Zeiss, Thornwood, NY). AFM probes used in our study include a silicon nitride sharp pyramidal tip and two different sizes of polystyrene spherical probes to determine the effect that tip geometry and size have on the measurements.

The pyramidal tip used, model Olympus TR400PSA (Asylum Research, Santa Barbara, CA), has a 20 nm nominal spherical cap radius, semiincluded angle (θ) of 36° (measured used scanning electron microscopy; see Fig. 1 *A*), mounted on a 200 μm triangular cantilever with nominal spring constant of 0.02 N/m. Spherical tips (Novascan Technologies, Ames, IA) used had nominal diameters of 4.5 (Fig. 1 *B*) and 10 μm mounted on a silicon nitride cantilever with nominal spring constant of 0.01 N/m. The spring constant was calibrated before each experiment using the Thermal Fluctuations function of the Nanoscope software that measures the cantilever's motion in response to thermal noise (23).

In a few experiments, a longer pyramidal tip was used to ensure that the underside of the cantilever was not affecting the measurements (11). We used a MPP-32100-10 (Bruker AFM Probes, Camarillo, CA) with a nominal front angle of 15°, side angle of 17.5°and back angle of 25°, and a tip radius of 8 nm. Its tip height was 15–20 μm as compared to 2.9 μm for the Olympus tip used. Unless otherwise mentioned in the text, all results presented for a sharp tip are for the Olympus tip.

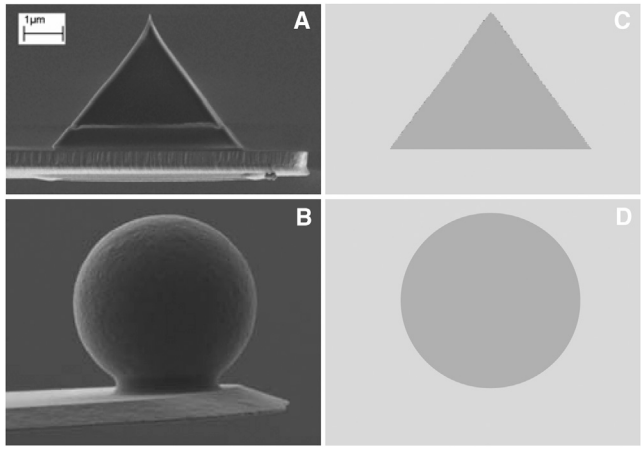

FIGURE 1 Scanning electron microscopy image of the sharp tip (*A*) and the spherical 4.5 μm tip (*B*). (*C* and *D*) Shape of the corresponding tip used in the finite element M modeling. All panels are at the same scale.

During AFM experiments, cells were maintained in culture medium at 37°C. Force measurements were made by indenting isolated cells up to 400 nm in depth; in one study with a sharp Bruker tip, the effects of deeper indentations (up to 900 nm) were examined. The tip velocity used during indentation (800 nm/s) was chosen to avoid viscous effects (4) based on preliminary studies. A total of 5–10 force measurements per cell were done at different locations including locations above the nucleus of the cell and in nonnuclear regions, avoiding the periphery of the cell.

The force (F) applied to indent the cell was determined as a function of indentation depth (δ). The former was found as $F = k(d-d_o)$, where k and d are the spring constant and deflection of the cantilever, respectively, and d_o is the deflection when contact is first established between the tip and the cell. The indentation was determined as $\delta = (z - z_o) - (d - d_o)$ where z is the height of the tip from an arbitrary datum and z_o is the height of the tip at the point of initial contact (7). The initial point of contact with the cell (z_o, d_o) was determined using an algorithm proposed by Crick and Yin (21) in which noise is accounted for by picking a best fit of pre- and post-contact data. Assuming that pre-contact data are linear and post-contact data are quadratic, the algorithm chooses the putative contact point as the one that produces the best fit for both pre-and post-contact data. Fig. 2, *A* and *B*, show typical results for F versus δ for the sharp and spherical tip, respectively.

To determine the aggregate cell modulus, a theoretical model relating F to δ was applied. For a pyramidal tip, the following relationship has been proposed (24) although it was not ultimately used in our studies (see below):

$$F = \frac{1.4906E\cdot\tan\theta}{2(1-\nu^2)}\cdot\delta^2. \quad (1)$$

For a spherical tip, we used the following relationship (25):

$$F = \frac{4E\cdot R^{\frac{1}{2}}}{3(1-\nu^2)}\cdot\delta^{\frac{3}{2}}. \quad (2)$$

In each case, the Poisson's ratio (ν) was set equal to 0.5, assuming cells are incompressible (11,26,27). For Eq. 1, $\theta = 36°$ (except for the longer Bruker tip where an angle of either 15° or 25° was used) whereas for Eq. 2, the radius of the spherical tip used (4.5 or 10 μm) was used for R. Typical

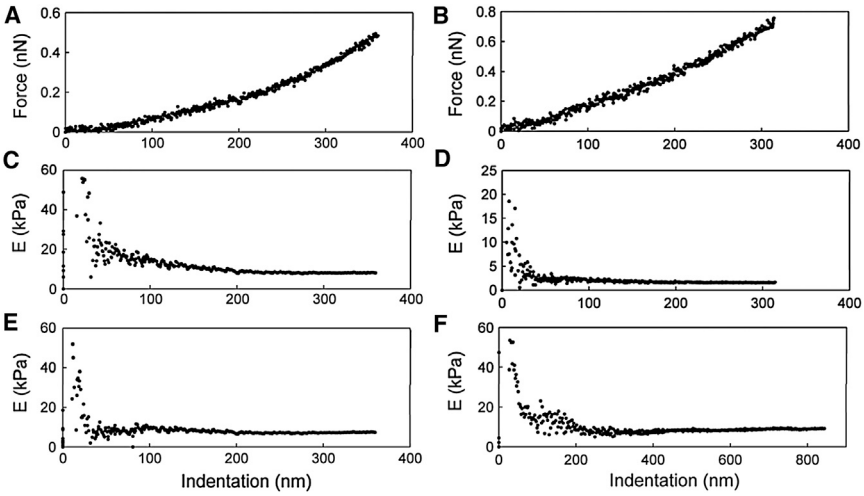

FIGURE 2 Sample of force-versus-indentation data measured on SC cells with AFM using (*A*) sharp and (*B*) 4.5 μm spherical tips. Corresponding values of Young's modulus were calculated for a sharp tip using Eq. 1 (*C*, for sharp tip), Eq. 2 (*D*, for 4.5 μm spherical tip), and Eq. 3 (*E*, for sharp tip). (*F*) Typical results for Young's modulus calculated using Eq. 3 for the longer Bruker sharp tip.

results are seen in Fig. 2, *C* and *D*. We note that ν in some cell types has been measured with values as low as 0.3 (28,29). Equations 1–3, used to experimentally calculate the cell modulus, each have an identical factor of $1–\nu^2$ in the expression relating force to indentation. Using a value of ν of 0.3 instead of 0.5 in these equations would increase the measured values of E by ~20%, but it would have the same effect on all measurements and thus, none of the relative comparisons would be affected.

Although the results from the spherical tip (e.g., Fig. 2 *D*) showed that E was relatively independent of δ (except for very small values of δ), this was not the case for the sharp tip (e.g., Fig. 2 *C*). These showed that E, as calculated using Eq. 1, decreased with increasing δ. Such behavior has been previously described by Rico et al. (13) and Briscoe et al. (30) for pyramidal and conical indenters, respectively. They noted that sharp tapered tips are not perfectly sharp but have a spherical cap at the apex. If a perfectly tapered geometry was assumed, an anomalous depth dependence of E was evident at moderate indentations. To correct for this, they developed the following model that behaves like a spherical tip for small indentations ($\delta < b^2/R$) and a tapered tip for larger deformations:

$$F = \frac{2E}{1-\nu^2}\left(a\delta - m\frac{a^2}{\tan\theta}\left[\frac{\pi}{2} - \sin^{-1}\left(\frac{b}{a}\right)\right] - \frac{a^3}{3R} + \left(a^2-b^2\right)^{\frac{1}{2}}\left[\frac{mb}{\tan\theta} + \frac{a^2-b^2}{3R}\right]\right), \tag{3a}$$

$$\delta - \frac{a}{R}\left[a - \left(a^2-b^2\right)^{\frac{1}{2}}\right] - \frac{na}{\tan\theta}\left[\frac{\pi}{2} - \sin^{-1}\left(\frac{b}{a}\right)\right] = 0, \tag{3b}$$

where $b = R\cos\theta$ and R is the radius of the spherical cap (20 nm for the Olympus tip; 8 nm for the Bruker tip). For a pyramidal tip, $m = 2^{1/2}/\pi$, and $n = 2^{3/2}/\pi$; for a cone, $m = 1/2$, and $n = 1$ (8). Using this model, E was found to be relatively constant for $\delta > 50$ nm or so (see typical example in Fig. 2 *E*). Based on these results, Eq. 2 was used to analyze data from spherical tips and for sharp tips at small indentations ($\delta < b^2/R$) whereas Eq. 3 was used for larger indentations (Eq. 1 was only used to generate Fig. 2 *C* and was not otherwise used in the results reported here).

In a few cells of each cell type, cell thickness was estimated for use in our modeling studies. The vertical position of the probe was determined when the tip first makes contact with the surface of the cell. After indentation measurements were completed, the tip was retracted and positioned next to the cell. Then the tip was moved down until contact was established with the culture dish. The difference in height between the culture dish and the surface of the cell was taken as an estimate of the cell thickness.

Finite element modeling methods

We modeled the process by which the AFM tip indented into the cell cortex and underlying internal cytoskeleton (see Fig. 6, *A* and *B*). The tip was modeled as a rigid body (16) with its geometry chosen to match the tips used during AFM experiments (Fig. 1, *C* and *D*). The geometry of the sharp tip was simplified from a pyramid to a cone to take advantage of the reduced computational cost that arises from using an axisymmetric model instead of a three-dimensional geometry.

The cytoskeleton of the cell was modeled as a cylindrical disk with a radius of 10 or 20 μm and thickness of 3 μm, with a cortex surrounding the cell having a thickness of 200–400 nm. The radius was chosen such that the strain at the edges of the domain was <0.1% of the strain near the tip. We verified that increasing the radius of the disk by twofold did not significantly affect the results (<1.25% difference). The thickness of the disk was chosen based on the average thickness of the cell as measured during AFM experiments. Increasing or decreasing the thickness of the disk by a factor of two had negligible effect on the results using the sharp tip model (<0.1%), and only a small/moderate effect on the results using the spherical tips (6% for increased thickness and up to 20% for decreased thickness). The cortex thickness was based on measurements using confocal microscopy, as described below.

The internal cytoskeleton (underlying the cortex) was assumed to be a homogeneous neo-Hookean material (32) with a modulus of 1 kPa (19). Although cells were assumed to be incompressible, a Poisson's ratio of 0.49 was used for numerical stability (33). The cortex was also modeled as an incompressible, homogeneous neo-Hookean material with a modulus that was varied from 1 to 100 times the modulus of the internal cytoskeleton. Previous estimates of cell cortex stiffness range from $E = 9$ to 4500 kPa (34). We also examined the effect on the strain distribution of lowering the Poisson's ratio to 0.3 in both internal cytoskeleton and cortex.

The basal surface of the cell was constrained to zero displacement. Zero relative displacement was assumed between the cortex and the underlying internal cytoskeleton (no-slip condition). No tractions forces were applied between the AFM tip and cortex (consistent with the theoretical models used for data analysis) and the apical surface of the cortex was assumed to remain in contact with the AFM tip throughout the deformation process (11). Zero stress was prescribed at the upper surface of the cortex not in direct contact with the AFM tip and the side edges of the domain were free to move.

Finite element modeling (FEM) studies were done using the software ABAQUS CAE (Ver. 6.7, Dassault Systèmes Simulia, Providence, RI). Quadrilateral, four-node bilinear elements were used to discretize the cortex and the internal cytoskeleton. Elements of 1 and 10 nm were used for the sharp and spherical tip model, respectively. The mesh was chosen by systematically reducing its size until the results were independent of element

size, while allowing a more refined mesh near the tip where larger deformations were expected. For the sharp tip model, the ALE adaptive meshing feature was used on the cortex and internal cytoskeleton to improve the aspect ratio of the mesh. Due to the high strains generated by this tip, an adaptive meshing feature was used that improved the quality of the mesh during large deformations by allowing the mesh to move independently of the material and prevented high distortion of the elements. The new position of a node was determined based on the average of the positions of each of the adjacent nodes by using the Laplacian smoothing method. An explicit method was used to solve for the stress, strain, and displacement fields as a function of indentation.

For each tip, we calculated the indentation force as a function of indentation depth. This force-deformation relation was then fitted by Eq. 2 (for spherical tip) or Eq. 3 (for sharp tip) to obtain an apparent Young's modulus, E_{apparent}, the equivalent modulus of a cell composed of a single uniform material. The vertical downward displacement of the indenter was limited to 80 nm. Higher indentations with a sharp tip caused excessive distortion of the elements and the model did not converge to a solution. Ng et al. (18) reported a similar limitation in their work modeling AFM indentations.

To validate FEM techniques, we compared the numerical results for E_{apparent} to a prescribed value of E for both a sharp tip and a spherical tip indenting a semiinfinite, homogenous, elastic medium of given modulus (E). Calculated values of E_{apparent} were within 0.5% of the given modulus in both cases.

Imaging studies

HUVEC and SC cells were grown on glass slides following the same procedures described above. They were then fixed in a solution of 10 mL paraformaldehyde 10% (Electron Microscopy Sciences, Harfield, PA) with 15 mL of Dulbecco's phosphate-buffered saline (Mediatech, Manassas, VA). After 1 h, fixative solution was replaced by buffer and the cells remained in buffer until use. Cells were stained with Alexa Fluor 488 phalloidin (Molecular Probes, Eugene, OR) for 20 min to stain for F-actin, and then washed and mounted using mount media with DAPI. The mounted slides were imaged with a LSM-700 confocal microscope (Carl Zeiss, Thornwood, NY). Z-stacks (each image at 0.17μm optical slice) were taken for randomly picked cells ($N = 5$ for each group) with a 63× oil objective at optimal resolution (2048 × 2048), zoom 0.7. The final stack was examined and processed for cross section by using a cut function in the ZeN2010 software (Carl Zeiss).

For measurements of cortex thickness in live cells, HUVEC and SC cells were transduced with an adenovirus delivering an actin filament marker, rAV-LifeAct-TagGFP2 (IBIDI, Verona, WI) (35). After 48 h of transduction, cells were washed with Dulbecco's phosphate-buffered saline and imaged with a structured illumination microscope (SIM) along the Z-stacks (thickness of 0.15 μm/slice) with excitation at 488 nm (Nikon, Melville, NY). A CFI Apo TIRF 100×-oil-immersion lens (NA = 1.49) was used (Nikon). The imaging was done for 10 HUVECs and 10 SC cells. For each cell, five cortex thickness measurements were made on the lateral aspect of the cell, well away from the top and bottom of the cell and well away from the front and back of the cell. Thickness measurements were made by taking an intensity profile perpendicular to the cortex at each location and then defining the thickness based on full width at half-maximum; we note that measurements based on counting illuminated pixels across the thickness of the cortex gave good agreement with this less subjective method of measurement.

Statistical methods

The statistical analysis was done using the software SPSS (Ver. 12.0, IBM, Somers, NY). Because the data sets were not normally distributed as determined using a Q-Q plot (36), a logarithmic transformation of the data was performed before determining data means and applying Student's t-tests. The log transformation resulted in the data being normally distributed. Log-transformed data were used to compute means, and significance was determined at the 0.05 level using an independent-sample Student's t-test not assuming equal variances. Data are reported as geometric means ± standard error about the geometric mean. It should be noted that the conclusions drawn from these data do not depend on use of the log transformation, other than the normality of the log data set. All statistically significant results were confirmed using a Mann-Whitney U-test.

RESULTS

Cell imaging

Imaging studies were done to establish that these cell types have a prominent cell cortex and to estimate the thickness of this cortex. Confocal reconstruction allowed us to visualize cross-section of these cells as shown in Fig. 3. F-actin staining showed a dense cortex on both the basal and apical aspect of these cells, consistent with a high cortical stiffness.

The cortex thickness was measured as 312 ± 65 nm (mean ± SE, $n = 50$) for the HUVEC and 371 ± 91 nm ($n = 50$) for the SC cells. The average value of the SC cells cortex thickness was significantly higher than that of the HUVECs ($p < 0.03$).

Imaging studies (Fig. 4) using SIM showed that use of Latrunculin-A entirely eliminated the cortex of both HUVEC and SC cells. These studies also showed that Latrunculin-A largely removed stress fibers and actin filaments from the internal cytoskeleton of SC cells. The effect on HUVEC was more variable, with filaments still apparent that may be remnants of stress fibers, albeit less prominent and much less organized than before Latrunculin-A treatment. A video (Movie S1) that dramatically shows the removal of the cell cortex by Latrunculin-A in an SC cell is found in the Supporting Material.

AFM measurements

Cell staining was shown to have no effect on the AFM measurements of cell mechanical properties. Using the sharp tip, the modulus in stained cells was 2.54 ± 1.02 (n = 21)

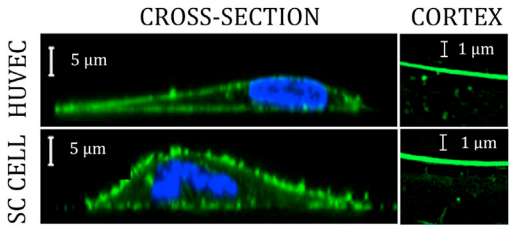

FIGURE 3 Confocal profile (0.17 μm per slice) of HUVEC and SC cell stained for F-actin (*green*, Alexa Fluor 488 Phalloidin) showing prominent cell cortex; images also show the cell nucleus (*blue*, DAPI). High-resolution images acquired using SIM (0.15 μm per slice) are shown of the cortex of HUVEC and SC cells labeled with an actin marker (LifeAct) that were used to measure the lateral cortex thickness. Fig. S2 (in the Supporting Material) shows a schematic of the locations on the cell where measurements of cortex thickness were typically made.

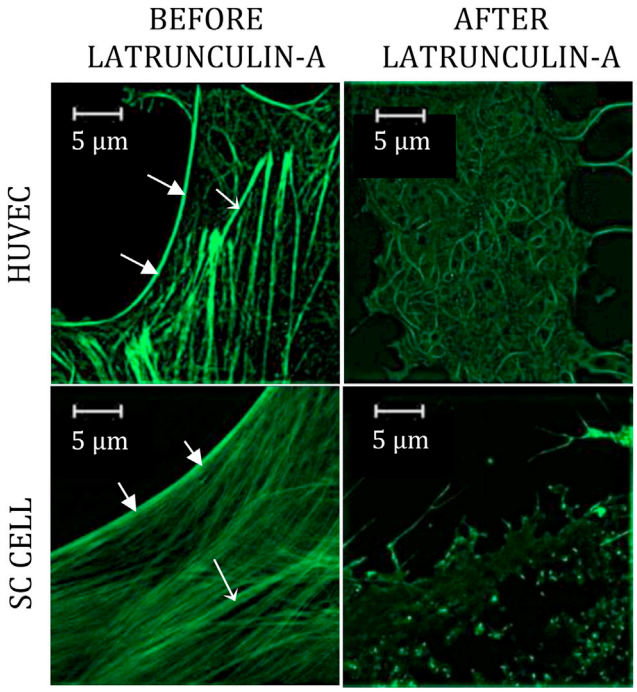

FIGURE 4 SIM images (0.15 μm per slice) of HUVEC and SC cell before and after treatment with Latrunculin-A (1 μM) for 30 min. Cell cortex (*Short thick arrows*) seen on cells before Latrunculin-A treatment but not after. Stress fibers (*Long thin arrows*) in cells. All images at same brightness and contrast settings.

whereas in unstained cells was 2.42 $\pm$ 0.43 ($n = 18$); the difference was not statistically significant ($p = 0.83$) Using the 4.5μm tip, the modulus in stained cells was 1.40 $\pm$ 0.33 ($n = 33$) whereas in unstained cells it was 1.60 $\pm$ 0.40 ($n = 27$) ($p = 0.55$).

In some cell stains, HUVEC and SC cells were probed in their nuclear and nonnuclear regions using the three different tips. The results are shown in Table 1. Measurements of modulus in the nuclear and nonnuclear regions were not statistically significantly different from one another ($p > 0.2$), except for the 10μm tip results in the SC cells ($p < 0.01$). However, even for the 10μm results, the magnitude of the difference between nuclear and nonnuclear regions was relatively small (<30%), and thus, data from these two regions were pooled in the other studies described below.

Significant differences in modulus were found among those measured with the sharp tip, the 4.5μm spherical tip, and the 10μm spherical tip in both HUVEC and SC cells (Fig. 5 *A*). The sharp tips gave the highest measurements with a modulus of 3.23 $\pm$ 0.54 kPa ($n = 49$) in the HUVEC and 6.67 $\pm$ 1.07 ($n = 104$) in the SC cells. These values were much higher ($p < 10^{-7}$) than measurements using the 4.5μm tip in HUVEC (1.00 $\pm$ 0.24, $n = 50$) and in SC cells (1.12 $\pm$ 0.12, $n = 104$). The values measured with the 4.5μm tip were in turn greater ($p < 10^{-3}$) than those measured with the 10μm tip in HUVEC (0.39 $\pm$ 0.07, $n = 28$) and in SC cells (0.84 $\pm$ 0.06, $n = 153$). The average values for all spherical tips were 0.71 $\pm$ 0.16 ($n = 78$) in HUVEC and 0.94 $\pm$ 0.06 ($n = 257$) in SC cells. SC cells were stiffer than HUVEC as measured with the sharp tip ($p < 10^{-5}$) and 10μm tips ($p < 10^{-6}$), but not significantly different for the 4.5μm tips ($p > 0.4$).

To ensure that the underside of the cantilever of the AFM tip was not affecting the measurements (11), we used a much longer sharp AFM tip (Bruker) to measure cell modulus in one SC cell strain (SC67) and compared those measurements to those made using the shorter Olympus tip in the same cell strain. The modulus calculated depends on which angle of the multiangled tip is used in Eq. 3 and thus, the minimum and maximum values were used to set a range. E for the Bruker tip was comparable but somewhat higher than modulus measured with the shorter Olympus tip. For the Bruker tip, E was found to be 11.0 $\pm$ 7.8 kPa ($n = 11$) as determined using a tip angle of 15° and 6.62 $\pm$ 4.62 kPa for an angle of 25° as compared to a mean value of 5.15 $\pm$ 2.06 kPa ($n = 18$) measured with the Olympus tip. The difference between the Bruker (using an angle of 15°) and the Olympus was not statistically significant ($p = 0.11$) but suggestive that the modulus measured by the Bruker tip was perhaps a little higher due to the smaller radius of curvature of its tip.

Because the moduli measured with sharp tips were much higher than those measured with the spherical tips, we examined to see if there was evidence that the cell stiffness increased with increased indentation depth. Results showed either a relatively constant modulus (e.g., Fig. 2 *E*) or decreasing modulus as the indentation increased. In one study using a sharp Bruker tip, we examined the effect of increasing the indentation up to 900 nm to determine

TABLE 1 Young's modulus (kPa) measured with AFM

		HUVEC		SC cells	
		Nucleus	Nonnuclear	Nucleus	Nonnuclear
Sharp tip	Mean $\pm$ SE	3.80 $\pm$ 0.5	3.96 $\pm$ 2.3	6.38 $\pm$ 1.64	7.02 $\pm$ 1.34
	Measurements	16	12	55	49
Spherical tip (4.5 μm)	Mean $\pm$ SE	0.47 $\pm$ 0.08	0.59 $\pm$ 0.12	1.19 $\pm$ 0.19	1.05 $\pm$ 0.13
	Measurements	11	6	52	52
Spherical tip (10 μm)	Mean $\pm$ SE	0.35 $\pm$ 0.05	0.54 $\pm$ 0.24	0.71 $\pm$ 0.08	0.96 $\pm$ 0.08
	Measurements	21	7	71	82

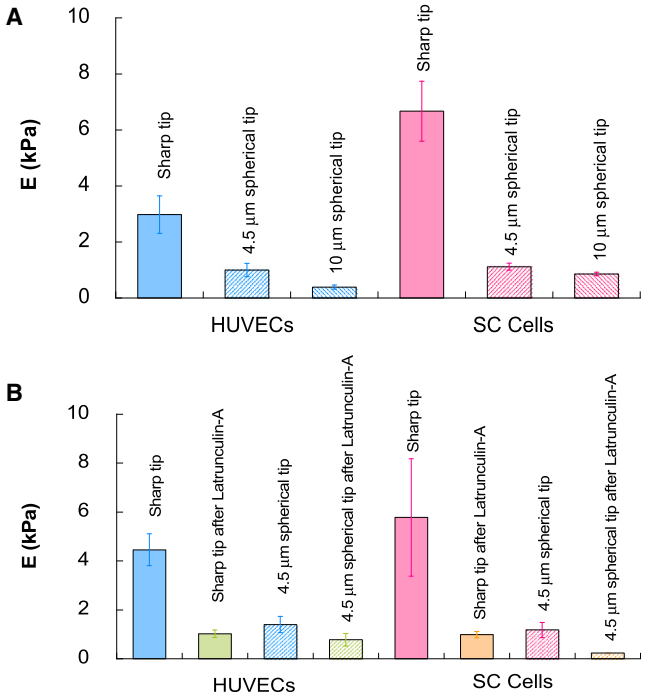

FIGURE 5 (*A*) Young's modulus (*E*) of HUVEC and SC cells (SC) as measured with AFM using sharp and spherical tips. (*B*) Effects of Latrunculin-A (1 μM) on cell modulus.

whether our conclusions for very shallow indentations would hold for deeper indentation. A comparison of Fig. 2 *E* to Fig. 2 *F* shows very similar behavior for indentations up to 400 nm with an Olympus sharp tip and that of a Bruker tip with indentations up to 900 nm.

Addition of Latrunculin-A to HUVECs and SC cells decreased cell modulus as measured with the sharp tip and that measured using a 4.5μm spherical tip (Fig. 5 *B*). In HUVEC, Latrunculin-A decreased *E* as measured with a sharp tip from 4.46 $\pm$ 0.65 kPa ($n = 57$) in control cell to 1.02 $\pm$ 0.15 kPa ($n = 25$) ($p < 10^{-14}$); for the spherical tip, Latrunculin-A decreased *E* from 1.40 $\pm$ 0.33 kPa ($n = 33$) to 0.78 $\pm$ 0.26 kPa ($n = 19$) ($p < 0.03$). For SC cells (SC67), Latrunculin-A decreased *E* as measured with a sharp tip from 5.78 $\pm$ 2.40 kPa ($n = 13$) in control cells to 0.99 $\pm$ 0.12 kPa ($n = 13$) ($p < 5 \times 10^{-5}$); for the spherical tip, Latrunculin-A decreased *E* from 1.18 $\pm$ 0.31 kPa ($n = 11$) to 0.24 $\pm$ 0.03 kPa ($n = 17$) ($p < 6 \times 10^{-6}$). Perhaps most importantly, Latrunculin-A decreased the ratio between the modulus measured with a sharp tip and that measured with a spherical tip. In HUVEC, this ratio was decreased from 3.18 before Latrunculin-A to 1.31 after Latrunculin-A; in SC cells, this ratio also decreased but less so, dropping from 4.90 to 4.22.

The average thickness of HUVEC and SC cells, as measured with AFM, was ~5 μm at the nucleus and 3 μm in the nonnuclear regions.

Finite element modeling results

Very different strains distributions were seen around the sharp tip as compared to the spherical tips, with much higher strains generated by the former. With a 400 nm cortex, the strain distribution for the sharp tip was localized within the cortex, in the vicinity of the tip, whereas for the spherical tip, the strain was spread throughout the cortex and internal cytoskeleton (Fig. 6) and the strain levels were much lower. This was also true for the 200 nm cortex, but somewhat high strain levels were seen in internal cytoskeleton (data not shown) for the sharp tip. Lowering Poisson's ratio from 0.5 to 0.3 had a significant effect on the strain distribution, decreasing the maximum strain by as much as 40% (data not shown). Strain increased roughly linearly with increasing indentation for both the spherical tip and the

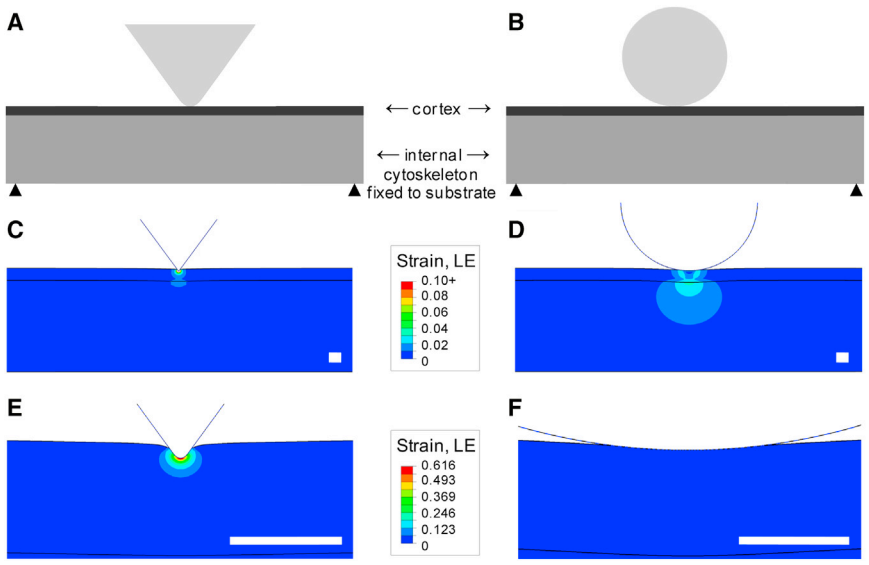

FIGURE 6 Schematic of the finite element model for sharp tip (*A*) or spherical tip (*B*). Strain distribution for the case when $E_{cortex}/E_{cytoskeleton} = 20$, cortex thickness = 400 nm, and $\nu = 0.49$. FEM results shown are the maximum logarithmic strain (LE) distribution in the cell after an 80 nm indentation using (*C*) sharp and (*D*) 4.5μm spherical tips. (*E* and *F*) Strain distribution in cortex for the sharp and 4.5μm spherical tips, respectively. (*Open scale bars*) 400 nm. Note that the strain scale is different in panels *C* and *D* as compared to panels *E* and *F*.

sharp tip (not shown); in the latter case, this was due to the rounded end of the sharp tip, as a truly sharp tip will give a different relationship for strain versus indentation (37).

To examine the effect of cortex stiffness on the AFM measurements, the stiffness of the cortex (E_{cortex}) was varied from 1 to 100 times the stiffness of the underlying internal cytoskeleton ($E_{cytoskeleton}$), while keeping all other parameters constant. When $E_{cortex} = E_{cytoskeleton}$, the apparent Young's modulus ($E_{apparent}$) was equal to that of the cortex and internal cytoskeleton (as expected), regardless of the tip geometry. As the cortex stiffness became stiffer than the internal cytoskeleton, $E_{apparent}$ was increased over the stiffness of the internal cytoskeleton. This increase was moderate for spherical tips (*open* and *solid circles* in Fig. 7, *A* and *B*) but dramatic for sharp tips (*triangles* in Fig. 7, *A* and B); these conclusions held for all cortex thicknesses investigated (200–400 nm). This confirmed that the sharp tips were much more affected by a relatively stiff cell cortex than were the spherical tips.

Because Poisson's ratio is not known for these cells, we examined its effects on $E_{apparent}$ by allowing it to vary between 0.3 and 0.49 (Fig. 7, *C* and *D*). The effect of Poisson's ratio was found to be modest for both sharp and spherical tips. Variations in cortex thickness had a much stronger effect, particularly for high values of $E_{cortex}/E_{cytoskeleton}$. An increase of cortex thickness from 200 nm to 400 nm led to as much as a 60% increase in $E_{apparent}$ for the sharp tip and more than a doubling for the spherical 4.5μm tip.

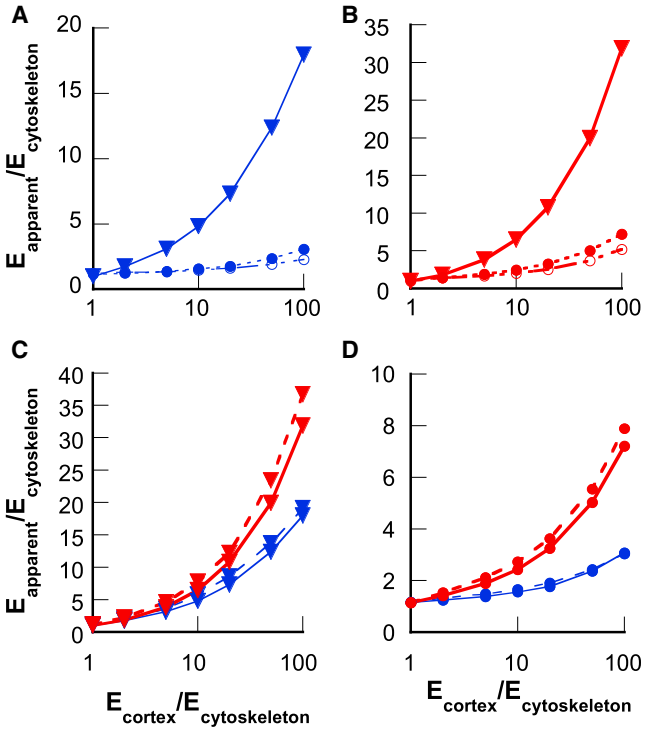

FIGURE 7 FEM results ($\nu = 0.49$) for $E_{apparent}/E_{cytoskeleton}$ as a function of cortex stiffness ($E_{cortex}/E_{cytoskeleton}$) calculated using a sharp tip (*triangles*), a 4.5μm spherical tip (*solid circles*), and a 10μm spherical tip (*open circles*) for a cortex thickness of 200 nm (*A*) and 400 nm (*B*). Effect of Poisson's ratio (ν) shown for sharp tips (*C*) and 4.5μm spherical tip (*D*) with $\nu = 0.49$ (*solid lines*) and $\nu = 0.3$ (*dashed lines*); (*thin/blue curves*) cortex thickness of 200 nm; and (*thick/red curves*) cortex thickness of 400 nm.

DISCUSSION

Our measurements of aggregate modulus in HUVEC were in the same range as measured in previous studies. With spherical tips, we measured a mean aggregate modulus of 0.71 kPa that was a little higher than the mean values of 0.35 kPa measured by Chouinard et al. (38) and similar to the value of 0.65–0.85 kPa measured by Stroka and co-workers (39–41). With a sharp tip, our values of aggregate modulus of 3.2 kPa are in reasonable agreement with mean values of 2.5–7 kPa measured by other groups (3,4,42,43). For SC cells, there are few studies for us to compare our results against. Our mean aggregate modulus of 0.94 kPa as measured using spherical tips is in the same range as that reported by Zeng et al. (19) (1–3 kPa) measured using magnetic pulling cytometry in central nonnuclear regions, but lower than their values in the nuclear region (4–8 kPa: we discuss this discrepancy later in this section). Our values were in the same range as reported by Zhou et al. (20) (0.5–1 kPa) measured using optical magnetic twisting cytometry. There are no comparable values to compare to for aggregate modulus of SC cells as measured with sharp tips.

It has been reported in previous studies (11–13) that AFM measurements using sharp pyramidal tips yield higher values of Young's modulus (E) than those using spherical probes. Our studies using both HUVEC and SC cells yielded similar results. We examined what might be the biophysical causes of the elevated modulus values that result from measurements using a sharp AFM tip.

Harris and Charras (11) showed that, for indentations that are greater than a critical value defined by the geometry of the sharp tip, it is possible for the cantilever to also be in contact with the cell. This would lead to an underestimation of the contact area of sharp tips and could explain why higher values of E are measured with pyramidal tips as compared to spherical tips. However, the range of indentations used in this study is well below that threshold. Furthermore, when we used a longer sharp tip (Bruker) to make these measurements (ruling out any possibility that the underside of the cantilever was affecting the measurements), equally high values were obtained.

Because the radius of sharp tips is much smaller than that of spherical tips, it has been suggested that sharp tips may cause strain hardening of the cell because of the high stresses and resulting strains generated (12). The strain hardening effect would cause E to increase with indentation (45) and perhaps explain the higher values measured with sharp tips. However, the modulus we measured using sharp tips did not increase with indentation depth over the range of

indentations studied (e.g., Fig. 2 *E*). This also rules out the possibility of a substrate effect on measurements made with the sharp tip, because it would also cause the modulus to increase with increasing deformation (4,46).

The cell cortex is an actin-dense region of the cell lying immediately beneath its plasma membrane. It is a porous network of cross-linked filaments, motors, and accessory proteins with a thickness between perhaps 100 and 400 nm in quiescent mammalian cells on a substrate (47). Because the stiffness of actin networks are strong functions of their actin concentration (48,49), this dense actin layer near the surface of the cell would be expected to be stiffer than the underlying cytoskeleton, and thus potentially might differentially affect AFM measurements, especially those using small indentations.

Confocal imaging showed that both HUVEC and SC cells have prominent cell cortices (Fig. 3) with thicknesses of ~300 and 375 nm, respectively. As this region would be expected to be stiffer than the underlying internal cytoskeleton due to its high actin density, it may have a significant effect on the modulus of these cells as measured by AFM. Finite element modeling indicated that sharp tips generate very high strains, and these strains are largely limited to the region of the cell cortex. In contrast, the strains generated by spherical probes are not only much lower, but also spread throughout the cell cortex and internal cytoskeleton. Based on the strain distribution, we expect sharp tips to be more sensitive than spherical tips to the stiffness of the cortex, particularly for the small indentations used in this study.

To determine if the higher values of Young's modulus measured with sharp tips might be, at least in part, due to the effect of the cell cortex, we used FEM studies to determine how the apparent modulus (E_{apparent}) varies as a function of cortex stiffness for each tip geometry. As the stiffness of the cortex was increased, the E_{apparent} obtained using the sharp tip increased significantly, showing that measurements made with sharp tips are strongly affected by the cell cortex. E_{apparent} obtained using the spherical tips also increased but to a much smaller extent (Fig. 7, *A* and *B*). Our results suggest that careful consideration should be given when interpreting AFM data to account for the effect of the cell cortex.

Further support for our conclusion that the cell cortex is responsible for the higher cell stiffness that we measured using a sharp tip is provided by our studies using Latrunculin-A, which would be expected to significantly affect the actin-rich cortex. In both HUVEC and SC cells, the cell stiffness as measured with a sharp tip was greatly reduced following Latrunculin-A treatment consistent with the role we have ascribed to the cell cortex (Fig. 5 *B*). Latrunculin-A treatment also reduced the ratio of the value of cell stiffness as measured with a sharp tip, as compared to a rounded tip. This ratio was greatly reduced by Latrunculin-A in HUVEC, whereas a much smaller reduction was seen in SC cells. This latter effect may be related to the stronger effect of Latrunculin-A seen on the internal cytoskeleton in the SC cells as compared to the HUVEC (Fig. 4). It should be noted that the Latrunculin-A concentration used in these studies (1 μM) was likely less than the concentration necessary to completely depolymerize the actin in these cells. When we used higher concentrations, we found that the cells lose their attachment to the substrate, making AFM measurements difficult.

One puzzling result was our finding that the modulus of the cell, measured either with a sharp tip or a rounded tip, was not statistically significantly different in the region over the cell nucleus from the rest of the cell. However, the nuclei of endothelial cells are thought to be significantly stiffer than the remainder of the cell (50). Data from other groups using AFM to measure endothelial cell stiffness comparing nuclear regions to other regions of the cell are conflicting. Three publications (3,51,52) indicate that the nuclear region of endothelial cells is less stiff than the more peripheral regions of the cell, four other publications suggest the opposite (4,42,53,54), and one study found no difference between nuclear and nonnuclear regions (38). It may be that shallow AFM indentations might be variably affected by the underlying nucleus depending on the depth of the nucleus in the cell.

Limitations

The FEM described here treats the cortex and underlying cytoskeleton as elastic solids. This is a considerable simplification because the internal cytoskeleton and cortex are comprised of intricate and dynamic viscoelastic networks of filaments, motors, and associated proteins. Nonetheless, much valuable information has been gleaned from the use of such models to begin to roughly characterize the mechanical behavior of such networks (16,18,55–58). Poroelasticity (59,60) and viscoelasticity (47) were also not included in our model. Future studies would benefit from including these effects.

Our model of the cortex does not separately consider that the restoring force includes both an elastic component and an active tension component. These are combined in our model into an effective elastic response (47) for ease of computation, but this limits our ability to separately sort out these influences. A model that included both of these components, along with studies that examine the effects of drugs interrupting one or both these, would allow a more detailed characterization of the stiffness characteristics of the cortex (61).We note that a model that included only a tensile component to describe the cell cortex would not be consistent with our experimental measurements, because such a model would predict that the AFM force-versus-deformation curve (e.g., Fig. 2, *A* and *B*) would be linear (62,63).

FEM results presented here were limited to an indentation depth of 80 nm, whereas the experimental results were

extended for several hundred nm. This numerical limitation was due to the very high strains generated by the sharp tips. Although it would have been preferable to use the model to examine higher indentations, the relatively constant modulus with increased indentation seen experimentally adds confidence to these results.

Conclusions

Based on the AFM results using Latrunculin-A, our imaging studies, and our FEM results, we conclude that the higher modulus obtained in AFM experiments using shallow indentations when sharp tips are used as compared to when larger spherical probes are used can be explained by the presence of a cell cortex much stiffer than the underlying internal cytoskeleton. Sharp tips probe primarily the cortex whereas larger round tips are influenced by the stiffness of both the cortex and the underlying cytoskeleton. Alternate explanation of this result that include strain hardening or the effects of a hard substrate underlying the cell seem unlikely as these effects would result in values of E that increase with indentation. That behavior is not consistent with our results for AFM showing that modulus was relatively independent of indentation depth. Our use of the longer Bruker tip allowed us to ensure that the underside of the cantilever was not affecting our measurements with the sharp tip. Our results suggest that when making AFM measurements of cell modulus, the effects of the cortex on this measurement should be considered.

SUPPORTING MATERIAL

Supplemental movie, figure, and legends are available at http://www.biophysj.org/biophysj/supplemental/S0006-3495(13)00617-6.

We thank Dr. W. Daniel Stamer (Duke University) for providing the SC cells and Ruiyi Ren (Boston University) for technical assistance in confocal microscopy. AFM experiments were performed in the NIFTI facility of the NUANCE Center at Northwestern University.

R.V.-P. and M.J. acknowledge support from the National Glaucoma Research program of the Bright Focus Foundation and from the National Institutes of Health grant No. R01 EY 01969. H.G. acknowledges support from National Institutes of Health grant No. R01 EY 01969 and The Massachusetts Lions Eye Research Fund, Inc., to Boston University. R.V.-P. acknowledges support from National Institutes of Health grant No. T32 EY007128. The NUANCE Center is supported by the National Science Foundation-Nanoscale Science and Engineering Center, the National Science Foundation-Materials Research Science and Engineering Centers, the Keck Foundation, the State of Illinois, and Northwestern University. Imaging studies were done at the Nikon Imaging Center, Feinberg School of Medicine, Northwestern University.

REFERENCES

1. Costa, K. 2006. Imaging and probing cell mechanical properties with the atomic force microscope. *In* Cell Imaging Techniques. D. Taatjes and B. Mossman, editors. Humana Press, Totowa, NJ. 331–361.
2. Kasas, S., X. Wang, …, S. Catsicas. 2005. Superficial and deep changes of cellular mechanical properties following cytoskeleton disassembly. *Cell Motil. Cytoskeleton.* 62:124–132.
3. Kataoka, N., K. Iwaki, …, F. Kajiya. 2002. Measurements of endothelial cell-to-cell and cell-to-substrate gaps and micromechanical properties of endothelial cells during monocyte adhesion. *Proc. Natl. Acad. Sci. USA.* 99:15638–15643.
4. Mathur, A. B., A. M. Collinsworth, …, G. A. Truskey. 2001. Endothelial, cardiac muscle and skeletal muscle exhibit different viscous and elastic properties as determined by atomic force microscopy. *J. Biomech.* 34:1545–1553.
5. Sato, H., N. Kataoka, …, T. Masuda. 2004. Kinetic study on the elastic change of vascular endothelial cells on collagen matrices by atomic force microscopy. *Colloids Surf. B Biointerfaces.* 34:141–146.
6. Radmacher, M. 1997. Measuring the elastic properties of biological samples with the AFM. *IEEE Eng. Med. Biol. Mag.* 16:47–57.
7. Weisenhorn, A. L., M. Khorsandi, …, H.-J. Butt. 1993. Deformation and height anomaly of soft surfaces studied with an AFM. *Nanotechnology.* 4:106–113.
8. Lin, D. C., E. K. Dimitriadis, and F. Horkay. 2007. Robust strategies for automated AFM force curve analysis. I. Non-adhesive indentation of soft, inhomogeneous materials. *J. Biomech. Eng.* 129:430–440.
9. Stolz, M., R. Raiteri, …, U. Aebi. 2004. Dynamic elastic modulus of porcine articular cartilage determined at two different levels of tissue organization by indentation-type atomic force microscopy. *Biophys. J.* 86:3269–3283.
10. Engler, A. J., L. Richert, …, D. E. Discher. 2004. Surface probe measurements of the elasticity of sectioned tissue, thin gels and polyelectrolyte multilayer films: correlations between substrate stiffness and cell adhesion. *Surf. Sci.* 570:142–154.
11. Harris, A. R., and G. T. Charras. 2011. Experimental validation of atomic force microscopy-based cell elasticity measurements. *Nanotechnology.* 22:345102.
12. Carl, P., and H. Schillers. 2008. Elasticity measurement of living cells with an atomic force microscope: data acquisition and processing. *Pflugers Arch.* 457:551–559.
13. Rico, F., P. Roca-Cusachs, …, D. Navajas. 2005. Probing mechanical properties of living cells by atomic force microscopy with blunted pyramidal cantilever tips. *Phys. Rev. E.* 72:021914.
14. Darling, E. M., M. Topel, …, F. Guilak. 2008. Viscoelastic properties of human mesenchymally-derived stem cells and primary osteoblasts, chondrocytes, and adipocytes. *J. Biomech.* 41:454–464.
15. Dimitriadis, E. K., F. Horkay, …, R. S. Chadwick. 2002. Determination of elastic moduli of thin layers of soft material using the atomic force microscope. *Biophys. J.* 82:2798–2810.
16. Costa, K. D., and F. C. Yin. 1999. Analysis of indentation: implications for measuring mechanical properties with atomic force microscopy. *J. Biomech. Eng.* 121:462–471.
17. Akhremitchev, B. B., and G. C. Walker. 1999. Finite sample thickness effects on elasticity determination using atomic force microscopy. *Langmuir.* 15:5630–5634.
18. Ng, L., H.-H. Hung, …, A. Grodzinsky. 2007. Nanomechanical properties of individual chondrocytes and their developing growth factor-stimulated pericellular matrix. *J. Biomech.* 40:1011–1023.
19. Zeng, D., T. Juzkiw, …, M. Johnson. 2010. Young's modulus of elasticity of Schlemm's canal endothelial cells. *Biomech. Model. Mechanobiol.* 9:19–33.
20. Zhou, E. H., R. Krishnan, …, M. Johnson. 2012. Mechanical responsiveness of the endothelial cell of Schlemm's canal: scope, variability and its potential role in controlling aqueous humor outflow. *J. R. Soc. Interface.* 9:1144–1155.
21. Crick, S. L., and F. C. P. Yin. 2007. Assessing micromechanical properties of cells with atomic force microscopy: importance of the contact point. *Biomech. Model. Mechanobiol.* 6:199–210.

22. Stamer, W. D., B. C. Roberts, …, D. L. Epstein. 1998. Isolation, culture, and characterization of endothelial cells from Schlemm's canal. *Invest. Ophthalmol. Vis. Sci.* 39:1804–1812.

23. Hutter, J. L., and J. Bechhoefer. 1993. Calibration of atomic-force microscope tips. *Rev. Sci. Instrum.* 64:1868–1873.

24. Bilodeau, G. G. 1992. Regular pyramid punch problem. *J. Appl. Mech.* 59:519–523.

25. Harding, J. W., and I. N. Sneddon. 1945. The elastic stresses produced by the indentation of the plane surface of a semi-infinite elastic solid by a rigid punch. *Math. Proc. Camb. Philos. Soc.* 41:16–26.

26. Sirghi, L., J. Ponti, …, F. Rossi. 2008. Probing elasticity and adhesion of live cells by atomic force microscopy indentation. *Eur. Biophys. J.* 37:935–945.

27. Costa, K. D. 2003–2004. Single-cell elastography: probing for disease with the atomic force microscope. *Dis. Markers.* 19:139–154.

28. Freeman, P. M., R. N. Natarajan, …, T. P. Andriacchi. 1994. Chondrocyte cells respond mechanically to compressive loads. *J. Orthop. Res.* 12:311–320.

29. Trickey, W. R., F. P. T. Baaijens, …, F. Guilak. 2006. Determination of the Poisson's ratio of the cell: recovery properties of chondrocytes after release from complete micropipette aspiration. *J. Biomech.* 39:78–87.

30. Briscoe, B. J., K. S. Sebastian, and M. J. Adams. 1994. The effect of indenter geometry on the elastic response to indentation. *J. Phys. D Appl. Phys.* 27:1156–1162.

31. Reference deleted in proof.

32. Yamada, H., N. Mouri, and S. Nobuhara. 2010. Three-dimensional morphometry of single endothelial cells with substrate stretching and image-based finite element modeling. *EURASIP J. Adv. Signal Process.* 2010:1–10.

33. Dassault Systèmes. 2007. ABAQUS Theory and Analysis User's Manual, Ver. 6.7. Simulia Corp., Providence, RI.

34. Dailey, H. L., L. M. Ricles, …, S. N. Ghadiali. 2009. Image-based finite element modeling of alveolar epithelial cell injury during airway reopening. *J. Appl. Physiol.* 106:221–232.

35. Riedl, J., A. H. Crevenna, …, R. Wedlich-Soldner. 2008. LifeAct: a versatile marker to visualize F-actin. *Nat. Methods.* 5:605–607.

36. Moore, D., G. McCabe, and B. Craig. 2009. Introduction to the Practice of Statistics. HW Freeman, New York.

37. Johnson, K. L. 1970. The correlation of indentation experiments. *J. Mech. Phys. Solids.* 18:115–126.

38. Chouinard, J. A., G. Grenier, …, P. Vermette. 2008. Oxidized-LDL induce morphological changes and increase stiffness of endothelial cells. *Exp. Cell Res.* 314:3007–3016.

39. Stroka, K. M., and H. Aranda-Espinoza. 2011. Effects of morphology vs. cell-cell interactions on endothelial cell stiffness. *Cell Mol. Bioeng.* 4:9–27.

40. Stroka, K. M., and H. Aranda-Espinoza. 2011. Endothelial cell substrate stiffness influences neutrophil transmigration via myosin light chain kinase-dependent cell contraction. *Blood.* 118:1632–1640.

41. Stroka, K. M., J. A. Vaitkus, and H. Aranda-Espinoza. 2012. Endothelial cells undergo morphological, biomechanical, and dynamic changes in response to tumor necrosis factor-α. *Eur. Biophys. J.* 41:939–947.

42. Mathur, A. B., G. A. Truskey, and W. M. Reichert. 2000. Atomic force and total internal reflection fluorescence microscopy for the study of force transmission in endothelial cells. *Biophys. J.* 78:1725–1735.

43. Oberleithner, H., C. Riethmüller, …, H. Schillers. 2006. Differential action of steroid hormones on human endothelium. *J. Cell Sci.* 119:1926–1932.

44. Reference deleted in proof.

45. Leporatti, S., A. Gerth, …, E. Donath. 2006. Elasticity and adhesion of resting and lipopolysaccharide-stimulated macrophages. *FEBS Lett.* 580:450–454.

46. Domke, J., and M. Radmacher. 1998. Measuring the elastic properties of thin polymer films with the atomic force microscope. *Langmuir.* 14:3320–3325.

47. Salbreux, G., G. Charras, and E. Paluch. 2012. Actin cortex mechanics and cellular morphogenesis. *Trends Cell Biol.* 22:536–545.

48. Janmey, P. A., S. Hvidt, …, T. P. Stossel. 1994. The mechanical properties of actin gels. Elastic modulus and filament motions. *J. Biol. Chem.* 269:32503–32513.

49. Gardel, M. L., J. H. Shin, …, D. A. Weitz. 2004. Elastic behavior of cross-linked and bundled actin networks. *Science.* 304:1301–1305.

50. Caille, N., O. Thoumine, …, J. J. Meister. 2002. Contribution of the nucleus to the mechanical properties of endothelial cells. *J. Biomech.* 35:177–187.

51. Sato, M., K. Nagayama, …, K. Hane. 2000. Local mechanical properties measured by atomic force microscopy for cultured bovine endothelial cells exposed to shear stress. *J. Biomech.* 33:127–135.

52. Ohashi, T., Y. Ishii, …, M. Sato. 2002. Experimental and numerical analyses of local mechanical properties measured by atomic force microscopy for sheared endothelial cells. *Biomed. Mater. Eng.* 12:319–327.

53. Miyazaki, H., and K. Hayashi. 1999. Atomic force microscopic measurement of the mechanical properties of intact endothelial cells in fresh arteries. *Med. Biol. Eng. Comput.* 37:530–536.

54. Mathur, A. B., W. M. Reichert, and G. A. Truskey. 2007. Flow and high affinity binding affect the elastic modulus of the nucleus, cell body and the stress fibers of endothelial cells. *Ann. Biomed. Eng.* 35:1120–1130.

55. Charras, G. T., and M. A. Horton. 2002. Determination of cellular strains by combined atomic force microscopy and finite element modeling. *Biophys. J.* 83:858–879.

56. Charras, G. T., P. P. Lehenkari, and M. A. Horton. 2001. Atomic force microscopy can be used to mechanically stimulate osteoblasts and evaluate cellular strain distributions. *Ultramicroscopy.* 86:85–95.

57. Mijailovich, S. M., M. Kojic, …, J. J. Fredberg. 2002. A finite element model of cell deformation during magnetic bead twisting. *J. Appl. Physiol.* 93:1429–1436.

58. Kang, I., D. Panneerselvam, …, C. M. Doerschuk. 2008. Changes in the hyperelastic properties of endothelial cells induced by tumor necrosis factor-α. *Biophys. J.* 94:3273–3285.

59. Charras, G. T., J. C. Yarrow, …, T. J. Mitchison. 2005. Non-equilibration of hydrostatic pressure in blebbing cells. *Nature.* 435:365–369.

60. Mitchison, T. J., G. T. Charras, and L. Mahadevan. 2008. Implications of a poroelastic cytoplasm for the dynamics of animal cell shape. *Semin. Cell Dev. Biol.* 19:215–223.

61. Tinevez, J.-Y., U. Schulze, …, E. Paluch. 2009. Role of cortical tension in bleb growth. *Proc. Natl. Acad. Sci. USA.* 106:18581–18586.

62. Rosenbluth, M. J., W. A. Lam, and D. A. Fletcher. 2006. Force microscopy of nonadherent cells: a comparison of leukemia cell deformability. *Biophys. J.* 90:2994–3003.

63. Krieg, M., Y. Arboleda-Estudillo, …, C. P. Heisenberg. 2008. Tensile forces govern germ-layer organization in zebrafish. *Nat. Cell Biol.* 10:429–436.